Journal of Applied Polymer Science

An integrated numerical study of coextrusion flow inside and outside the die

Chuan Yang, Ziran Li
CAS Key Laboratory of Mechanical Behavior and Design of Materials, Department of Modern Mechanics, University of Science and Technology of China, Hefei 230027, China
Correspondence to: Z. Li (E-mail: lzr@ustc.edu.cn)

ABSTRACT: The three-dimensional coextrusion flow of two polymer melts is solved over the die-extrudate region using the finite element method. As elastic recovery is known to be the main source of extrudate swelling, a viscoelastic constitutive model (the Phan-Thien-Tanner or PTT model) is adopted to characterize the rheological behavior of the elastomers. A major challenge in the simulation of multilayer flow inside and outside the die is to update multiple moving surfaces (material interface and extrudate free surface) simultaneously. This difficulty is resolved by introducing a two-step updating algorithm which decouples the iterations of the interface and the free surface. The effects of extrudate swelling and bending on interface deformation are investigated herein, together with the interface shape dependency on flow elasticity. The numerical method is also applied to an industrial profile and the simulation result is in quantitative agreement with the experimental coextrusion data. © 2016 Wiley Periodicals, Inc. J. Appl. Polym. Sci. **2016**, *133*, 43522.

KEYWORDS: extrusion; surfaces and interfaces; swelling; theory and modeling; viscosity and viscoelasticity

Received 12 October 2015; accepted 5 February 2016
DOI: 10.1002/app.43522

INTRODUCTION

Multilayer coextrusion is a process in which two or more layers of different materials are extruded and joined together through a common die. By combining unique physical characteristics of each component (e.g., wear resistance, air-tightness, stiffness, adhesion, etc.), the coextrusion process can enhance the performance of resultant products at minimal cost. After decades of investigation and improvement, it has become a widely used manufacturing method in polymer industry. Compared with single-layer extrusion, multilayer coextrusion is a more complex process. The quality of extrudate product is affected by the extrudate swell phenomenon as well as the interface deformation between different layers. Therefore, a better understanding of the multiphase stratified flow in coextrusion process will benefit both the die design and the optimization of process parameters.

Early experimental studies on bicomponent coextrusion of polymer melts[1–5] showed that the viscosity difference between the two components is a controlling factor of the encapsulation phenomenon while elasticity is responsible for unstable or ragged interface shapes. Lee and White[3] pointed out that the existence of extrudate swell has a great influence on interface distortion and makes the interface shape observed in a cooled extrudate dissimilar from that within the die. In addition, Southern and Ballman[4] observed the exit angle of the extrudate stream and found that the extrudate tends to bend towards the slower moving component. This bending phenomenon also affects the final interface shape, as reported by Everage.[5]

As a complement to experimental studies, numerical simulation provides a useful tool to analyze the coextrusion process. A number of numerical methods have been proposed on the simulation of coextrusion flow inside the die. Takase *et al.*[6] performed a three-dimensional finite element simulation for viscoelastic bi-layer flow in a square die and showed that not only viscosity ratio but also elastic properties affect the encapsulation phenomenon. Anderson *et al.*[7] adopted the mapping method to determine interface location for coextruded polymer melts as they flow through channels with different geometries. It can be concluded from the results that, for viscoelastic fluids in noncircular channels, the secondary flow is a significant driving force for the deformation of layer interface. Gupta[8,9] proposed a mesh partitioning technique so that the finite element mesh can keep unaltered as the interface shape is developed during the simulation. The advantage of this technique is that it can be applied to simulate multilayer flows in dies with complex geometries. Under a quasi-two-dimensional hypothesis which excludes viscous encapsulation, Yue *et al.*[10] studied the elastically driven encapsulation in bicomponent stratified flow

using a phase-field method. The results indicated that the more elastic component tends to protrude into the other at the center of the duct and become encapsulated. Borzacchiello *et al.*[11,12] extended the phase-field formalism to fully three-dimensional computations and demonstrated that the viscosity or elasticity ratio alone cannot always predict the right encapsulation, while the real criterion is the jump of the second normal stress difference across the interface. It is worth mentioning that in most experimental works, the interface shapes were examined by photographing the cross sections of extrudate samples[1–5] while in the numerical simulations above, the interface shapes were investigated only at the die exits since the extrudate section was neglected. As a result, the influences of extrudate swell and bending on interface distortion could not be considered.

On the other hand, although the coextrusion flow outside the die is critical in determining the final interface curvature, it is much less studied. Main difficulties arise from the extrudate swell and the consequent deformation of the layer interface.[13] Karagiannis *et al.*[14] divided the coextrusion process into two stages and modeled each stage separately. The first stage consists of the stratified flow inside the die while the second stage involves the extrudate jet. The linkage between the two stages is the identical fully developed velocity profile imposed at the die exit. In agreement with previous experimentations,[4,5] extrudate bending was found in the second stage simulation. However, it should be noted that this modeling approach is only applicable to purely viscous constitutive models, like the Carreau model they employed. For viscoelastic fluids, due to the presence of memory effect,[15] the velocity boundary condition assigned at the die exit is inadequate to determine the elasticity level of the fluids which means the two stages cannot be properly linked. Therefore, in order to incorporate the effect of flow elasticity, which plays an important role in extrudate swell, the coextrusion flow over the die-extrudate region needs to be solved in one single model. However, to the authors' knowledge, such numerical studies have never been reported due to the difficulties inherent in the simulation.

In the present paper, we try to investigate the coextrusion flow of two polymer melts over the entire die-extrudate region by a three-dimensional finite element simulation. A two-step algorithm is proposed to decouple the update of the interface and the free surface. A 5-mode Phan-Thien-Tanner (PTT) model is employed to describe the viscoelastic behavior of polymeric fluids. The influences of extrudate distortion and flow elasticity on interface configuration are examined, respectively. To verify the validity of the numerical method, the bicomponent coextrusion of an industrial profile is simulated and compared with experimental observation.

NUMERICAL METHODS

Governing Equations

The numerical simulation is based on the following assumptions: (1) the fluids are incompressible and immiscible; (2) the flow is steady state and isothermal; (3) inertia, gravity and surface tension are neglected because of the high viscosity of molten polymers. Flow in the computational domain is governed by the equations of continuity and momentum, written as

$$\nabla \cdot \mathbf{v} = 0 \tag{1}$$

$$-\nabla p + \nabla \cdot \boldsymbol{\tau} = 0 \tag{2}$$

where $\mathbf{v}$ is the velocity vector, p is the pressure and $\boldsymbol{\tau}$ is the extra stress tensor.

The rheological properties of the polymer melts is described by the 5-mode Phan-Thien-Tanner (PTT) model,[16] expressed as

$$\begin{cases} \boldsymbol{\tau} = \sum_{i=1}^{5} \boldsymbol{\tau}^{(i)} \\ \exp\left[\frac{\varepsilon_i \lambda_i}{\eta_i} \mathrm{tr}(\boldsymbol{\tau}^{(i)})\right] \boldsymbol{\tau}^{(i)} + \lambda_i \left[\left(1 - \frac{\xi_i}{2}\right) \boldsymbol{\tau}^{(i)\nabla} + \frac{\xi_i}{2} \boldsymbol{\tau}^{(i)\overset{\Delta}{}}\right] = 2\eta_i \mathbf{D} \end{cases} \tag{3}$$

where the rate of deformation tensor is given by $\mathbf{D} = \frac{1}{2}\left(\mathbf{L} + \mathbf{L}^{\mathrm{T}}\right)$, with the velocity gradient tensor $\mathbf{L} = (\nabla \mathbf{v})^{\mathrm{T}}$, λ_i is the relaxation time, η_i is the zero shear viscosity, ε_i and ξ_i are parameters controlling the extensional viscosity and the second normal stress difference, respectively. The PTT model is capable of modeling the realistic extrudate swell effect as well as a nonzero second normal stress difference.[17–19]

To solve the governing equations, eqs. (1)–(3), at high levels of flow elasticity, the streamline upwind (SU) and the elastic viscous stress splitting (EVSS) formulations[20] are adopted. In the EVSS formulation, the viscoelastic stress is split into

$$\boldsymbol{\tau} = \boldsymbol{\tau}^{\mathrm{e}} + \boldsymbol{\tau}^{\mathrm{v}} \tag{4}$$

where $\boldsymbol{\tau}^{\mathrm{e}}$ denotes the elastic part of the extra stress tensor and

$$\boldsymbol{\tau}^{\mathrm{v}} = 2\eta \mathbf{D} \tag{5}$$

represents the viscous part. This stress splitting makes the momentum equation explicitly elliptic and stabilizes the numerical simulation of viscoelastic flow at high Weissenberg numbers (Wi).

Boundary Conditions

The coextrusion flow of two polymer melts consists of the merging of two fluid streams, the stratified flow within the die and the extrudate jet outside the die, as schematically shown in Figure 1. Due to symmetry of the system, only half of the domain is analyzed. Along the inlet boundaries of both fluids, fully developed velocity profiles are assigned. No-slip conditions are adopted at the die wall and the separation plate. Zero normal and tangential stresses are imposed at the far downstream of the extrudate. The conditions which have to be satisfied at the layer interface are kinematic conditions

$$\mathbf{n} \cdot \mathbf{v} = 0 \tag{6}$$

$$\mathbf{v}_{\mathrm{I}} = \mathbf{v}_{\mathrm{II}} \tag{7}$$

and dynamic conditions

$$\boldsymbol{\sigma}_{\mathrm{I}} = \boldsymbol{\sigma}_{\mathrm{II}} \tag{8}$$

where $\mathbf{n}$ is the unit normal vector, $\boldsymbol{\sigma}$ is the total stress tensor at the interface. Indices I and II refer to the upper layer (fluid I) and the lower layer (fluid II), respectively. Equation (6) requires that there is no flow across the interface while eqs. (7) and (8) ensure the continuity of velocities and the balance of stresses. In the absence of surface tension, zero normal and tangential

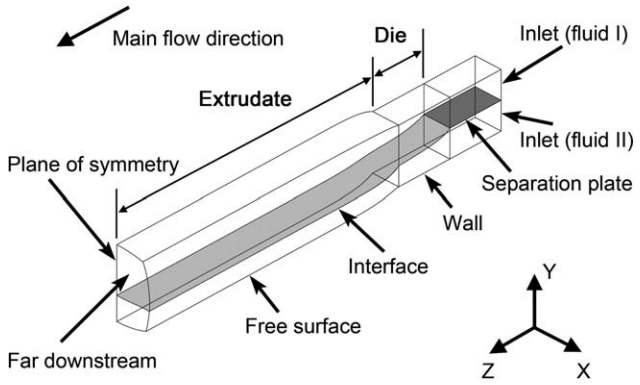

Figure 1. Schematic diagram of the bicomponent coextrusion flow.

stresses are considered on the free surface, together with the kinematic condition expressed by eq. (6).

Interface and Free Surface Update Schemes

Positions of the layer interface and the extrudate free surface are not known a prior and have to be determined as part of the solution. The streamline method is used to relocate these moving surfaces after each iteration step of the velocity field. The interface is described by a group of streamlines starting from the end of the separation plate (the line AB in Figure 2) while the free surface is represented by streamlines from the edge of the die exit (the lines CD, DF and FG in Figure 2). As the streamlines should be tangential to the velocity vector of the flow, we write

$$\frac{dx}{u}=\frac{dy}{v}=\frac{dz}{w} \tag{9}$$

from which we deduce

$$x=x_0+\int_{z_0}^{z}\frac{u}{w}dz \tag{10}$$

$$y=y_0+\int_{z_0}^{z}\frac{v}{w}dz \tag{11}$$

where u, v, and w are the velocity components in x, y and z directions, respectively. x_0, y_0 and z_0 are coordinates of the starting point. Based on eqs. (10) and (11), all the streamlines on the interface and the free surface can be updated.

The above approach is simple but adequate for the calculations of moving surfaces.[14,21] However, since the coextrusion flow is analyzed over the entire die-extrudate region in the present study, a difficulty arises from the simultaneous update of the interface and the free surface. According to eqs. (9)–(11), the locating of a new streamline needs a fixed starting point or, in other words, the coordinates of the starting point are boundary

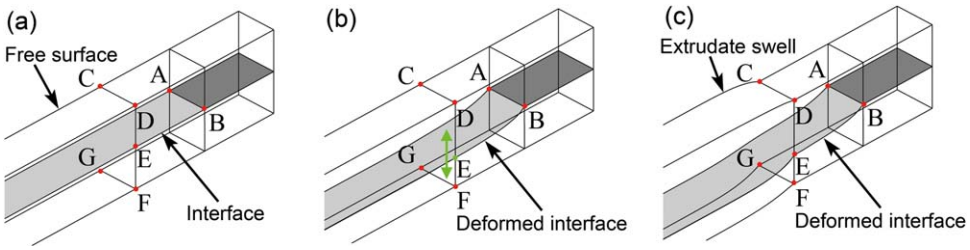

Figure 2. Update schemes for the interface and the free surface: (a) initial shapes of the moving surfaces; (b) deformed interface after the first updating step; (c) bilayered extrudate swell after the second updating step. [Color figure can be viewed in the online issue, which is available at wileyonlinelibrary.com.]

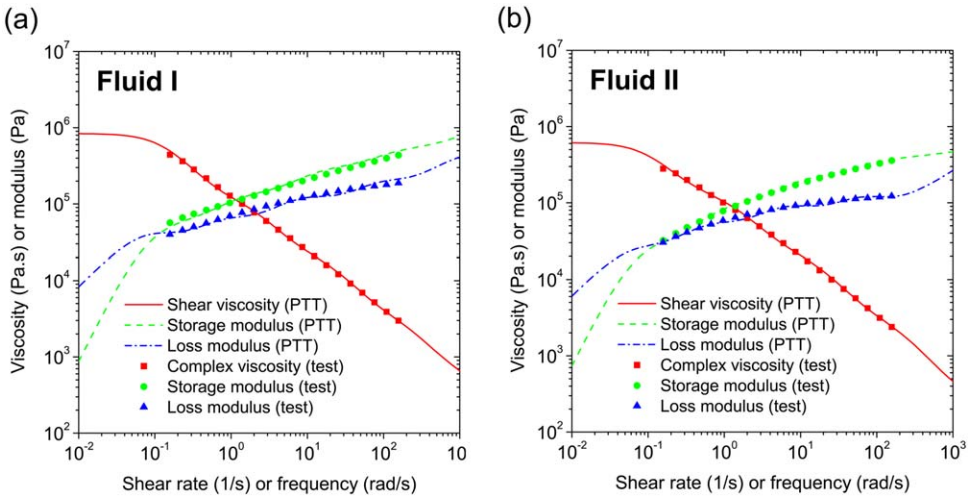

Figure 3. Rheology of the rubber compounds at 100 °C: (a) Fluid I; (b) Fluid II. [Color figure can be viewed in the online issue, which is available at wileyonlinelibrary.com.]

Table I. Material Parameters of the 5-mode PTT Model

Fluid I				
Mode no.	λ_i (s)	η_i (Pa.s)	ε_i	ξ_i
1	0.001	607.3481	0.011	0.227
2	0.010	2556.049	0.011	0.080
3	0.110	18282.04	0.026	0.074
4	1.147	90839.74	0.011	0.070
5	12.00	727133.4	0.038	0.131

Fluid II				
Mode no.	λ_i (s)	η_i (Pa.s)	ε_i	ξ_i
1	0.002	364.0922	0.011	0.228
2	0.015	2462.510	0.011	0.041
3	0.150	19121.41	0.025	0.063
4	1.500	103730.7	0.026	0.091
5	15.00	490636.1	0.038	0.161

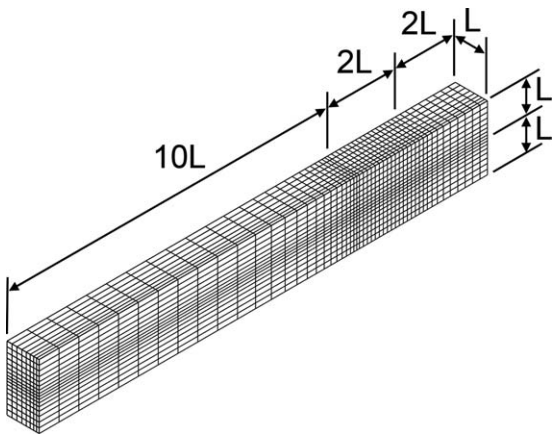

Figure 4. The finite element mesh used in the numerical simulation.

conditions which guarantee a unique and well-posed solution to eq. (9). As a result, nodal points on the lines AB, CD, DF and FG in Figure 2(a) are fixed during the simulation. This is inappropriate because the point E on the line DF needs to be relocated as part of the interface.

To resolve this contradiction, we divide the updating procedure into two steps. In the first step, the extrudate surface is not treated as a free surface but a free-slip wall where tangential (shear) stresses and normal velocities are set to zero. In doing so, the deformation of the extrudate surface is artificially suppressed so that only the layer interface is updated and the point E can be relocated along the line DF, as schematically shown in Figure 2(b). The second step is based on the deformed mesh of the previous step. Both the layer interface and the extrudate surface are defined as moving boundaries. The resultant swell of the bicomponent extrudate is depicted in Figure 2(c). To determine the final shapes of the interface and the free surface, the two-step iteration cycle can be repeated until convergence occurs, that is, the position of the point E does not change any more.

It should be admitted that the above updating algorithm tends to increase the computational cost. Fortunately, the convergence is faster than what we have expected. For the square die used in this study, a satisfactory level of convergence can be reached by repeating the updating procedure just three to four times.

RESULTS AND DISCUSSION

Numerical analysis of the above model is implemented in a finite element package Polyflow®.[22] The rheological data of two rubber compounds at 100 °C are adopted here to determine the parameters in the PTT model [eq. (3)]. Detailed information about the compounds and the rheological measurements can be found in our previous paper.[23] The PTT model fits the data well over a wide range of shear rates and frequencies, as presented in Figure 3 and Table I. It is worth mentioning that the upper limit of the validated shear rate range, 1.57×10^2 1/s, is high enough to cover the maximum shear rate in the numerical work. Due to the difficulties inherent to the rheological

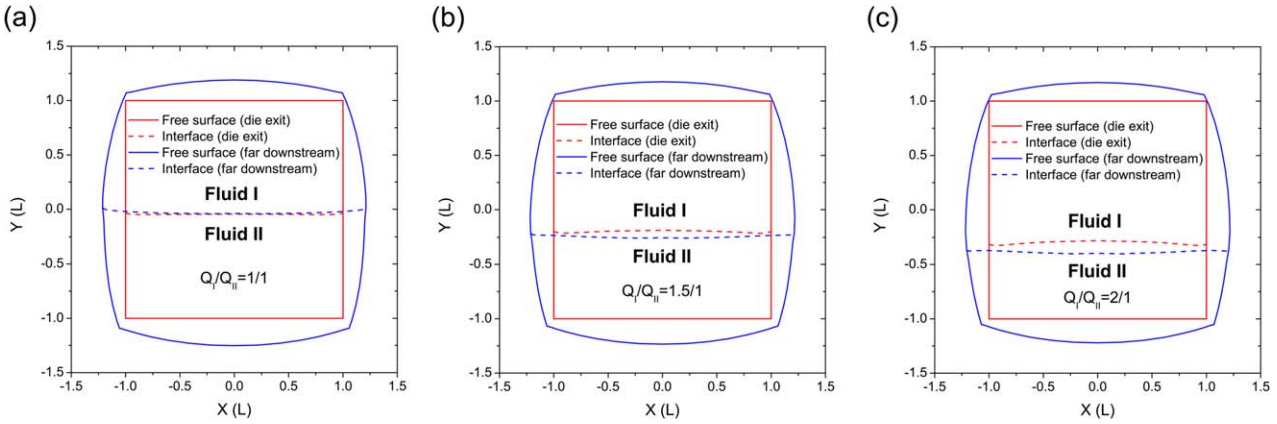

Figure 5. Comparison of moving surface profiles at the die exit and those at the far downstream with a fixed total volumetric flow rate QI + QII = 3 × 10-6 m3·s-1: (a) volumetric flow rate ratio QI / QII = 1 / 1; (b) QI /QII = 1.5 / 1; (c) QI / QII = 2 / 1. [Color figure can be viewed in the online issue, which is available at wileyonlinelibrary.com.]

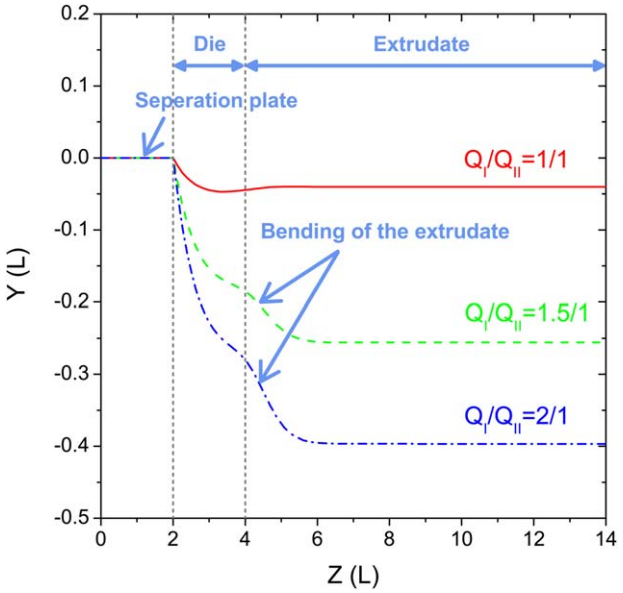

Figure 6. Center lines of the layer interface for different volumetric flow ratios (QI / QII) with a fixed total volumetric flow rate QI + QII = 3 × 10^{-6} $m^3 \cdot s^{-1}$. [Color figure can be viewed in the online issue, which is available at wileyonlinelibrary.com.]

measurements of filled elastomers,[24–26] the lower limit of the validated range reaches only 1.57×10^{-1} 1/s. We have to admit that, within the computational domain, there are regions in which the shear rates could be lower than this value. However, since the Weissenberg numbers (*Wi*) corresponding to these weak shear regions are relatively small, minor deviations of rheological properties do not have a significant impact on the overall elastic recovery of the extrudate.[27,28] Therefore, the extrapolation of rheological curves at vanishing shear rates in Figure 3 is considered to be reasonable for the simulation.

The mesh used in our computations consists of 6,528 hexahedral elements, with fine grids deployed near the die exit and the

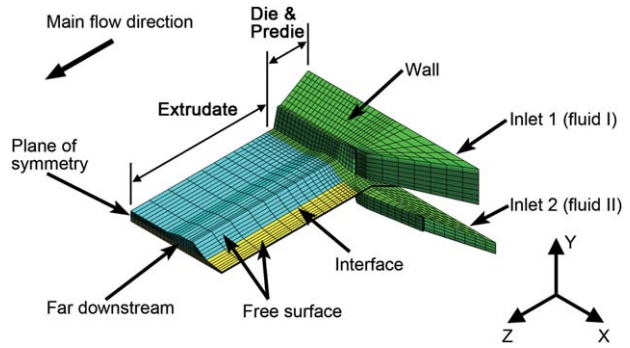

Figure 8. Computational domain for the coextrusion flow of the industrial profile. [Color figure can be viewed in the online issue, which is available at wileyonlinelibrary.com.]

interface, as shown in Figure 4 (the length L is set to 0.05 m). Mesh refinement has been checked to guarantee that the finite element solution is mesh-independent.

Effect of Swelling and Bending of the Extrudate

Previous experimental investigations[3–5] have pointed out that the extrudate swell effect and the bending are critical in determining the final interface shape. Here, we attempt to confirm this idea by comparing the interface profiles at the far downstream of the extrudate with those at the die exit. In the analysis, total volumetric flow rate (Q_I+Q_{II}) is set to 3×10^{-6} $m^3 \cdot s^{-1}$ and three different flow rate ratios (Q_I/Q_{II}), 1/1, 1.5/1 and 2/1, are considered.

As can be seen from Figure 5, owing to the extrudate swell, the interface profiles at the far downstream are remarkably stretched and become wider (over 20%) than the profiles at the die exit. In Figure 5(a) where $Q_I/Q_{II}=1/1$, the position and curvature of the interface at the far downstream is similar to those at the die exit. The lower layer (fluid II) tends to encapsulate the upper layer (fluid I) at both the far downstream and the die exit, although the encapsulation degree is slight. More appreciable encapsulation can be simulated by increasing the difference

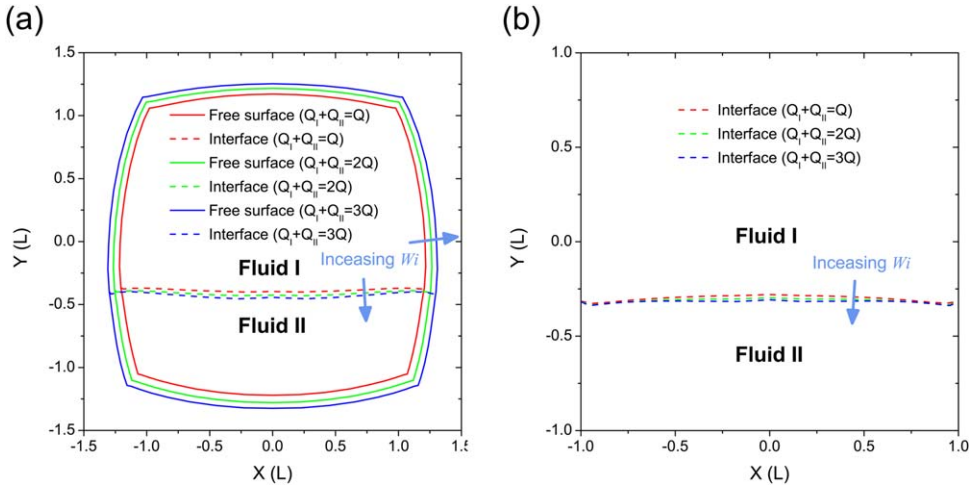

Figure 7. Interface and free surface profiles for different total volumetric flow rates (QI + QII) with a fixed volumetric flow rate ratio QI/QII = 2 / 1: (a) at the far downstream; (b) at the die exit. [Color figure can be viewed in the online issue, which is available at wileyonlinelibrary.com.]

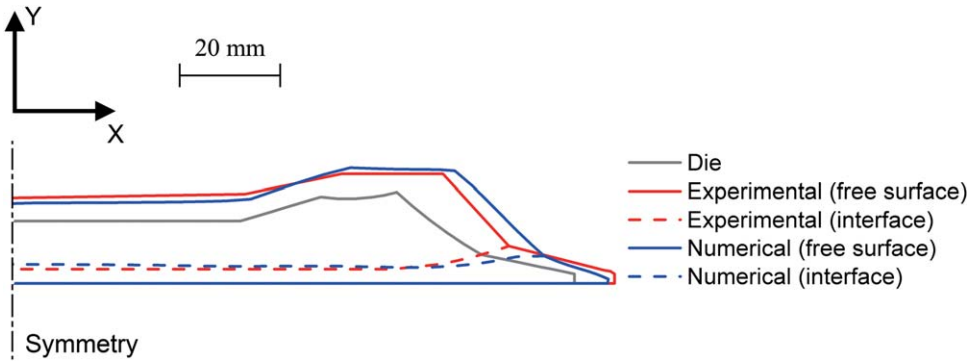

Figure 9. Comparison between the experimental extrudate profile and the numerical result. [Color figure can be viewed in the online issue, which is available at wileyonlinelibrary.com.]

of rheological behavior between the two components or extending the length of the die,[14] but that is an issue beyond the scope of the present paper. With the increase of flow rate ratio, the interface profile at the far downstream progressively deviates from the profile at the die exit, as presented in Figure 5(b,c). It should be noted that, for $Q_I/Q_{II}=1.5/1$ and $Q_I/Q_{II}=2/1$, the lower layer tends to encapsulate the upper layer at the far downstream, while at the die exit, the encapsulation is in the opposite direction, i.e., the upper tends to wrap around the lower. Consequently, we argue that the final interface shape of the extrudate cannot be directly extrapolated from the interface shape at the die exit.

Figure 6 illustrates how the center line of the layer interface (the intersection of the interface and the symmetric plane) alters its shape with the variation of volumetric flow rate ratio. For $Q_I/Q_{II}=1/1$, the center line is almost a straight line after leaving the die exit. In contrast, for the unequal component throughputs ($Q_I/Q_{II}=1.5/1$ and $Q_I/Q_{II}=2/1$), significant bending can be observed near the die exit. Thus, we believe the reversal of encapsulation direction shown in Figure 5(b,c) is associated with the bending of the extrudate stream, while the specific mechanism of this reversal could be complex and needs to be further studied.

Effect of Flow Elasticity

As the elasticity of polymer melts plays an important role in the extrudate swell phenomenon, we now examine how the elasticity level or the Weissenberg number (Wi) affects the shapes of the extrudate free surface and the layer interface. With a fixed flow rate ratio $Q_I/Q_{II}=2/1$, the total volumetric flow rate (Q_I+Q_{II}) is changed for $3\times10^{-6}\,m^3\cdot s^{-1}$ (Q), $6\times10^{-6}\,m^3\cdot s^{-1}$ ($2Q$) and $9\times10^{-6}\,m^3\cdot s^{-1}$ ($3Q$) in order to represent different levels of flow elasticity. Referring to Figure 7(a), the expansion of the free surface increases as the volumetric flow rate or the Weissenberg number (Wi) grows. The interface at the far downstream is also extended due to the overall extrudate swell while its curvature shows no significant change. At the die exit, one can see from Figure 7(b) that the middle part of the convex interface moves downward with increasing levels of flow elasticity while the endpoints remain in the same position. In other words, the interface tends to become flatter. Thus, it can be inferred from the results that the variation of flow elasticity has an influence on both the extrudate swell and the interface deformation.

EXPERIMENTAL

In order to verify the validity of the numerical method proposed above, a bicomponent coextrusion model is built for an industrial profile (Figure 8) and the result is accordingly compared with experimentation. Due to symmetry, only half of the system is analyzed. Boundary conditions are generally identical to those of the model shown in Figure 1. The total volumetric flow rate is set to $Q_I+Q_{II}=2.88\times10^{-6}\,m^3\cdot s^{-1}$ and the flow rate ratio of the two layers is fixed at $Q_I/Q_{II}=3.5/1$, which is consistent with the experimental setting. The 5-mode PTT model described by eq. (3) is also adopted here to characterize the rheology of the two rubber compounds at 100 °C and material parameters can be found in Table I as well.

Figure 9 shows the comparison between the numerical prediction of the extrudate profile and the experimental data. The shapes of the free surface and interface calculated by the simulation are in good agreement with the experimental observation. Even though this is a complex industrial profile, the numerical model is able to quantitatively predict the overall swelling of the extrudate jet as well as the curvature of the layer interface.

CONCLUSIONS

In the present study, the three-dimensional finite element method is employed to analyze the coextrusion flow of two rubber compounds over the die-extrudate region. A decoupled updating algorithm is proposed to relocate the positions of the layer interface and the extrudate free surface and a multimode Phan-Thien-Tanner (PTT) model is adopted to describe the realistic rheological behavior of the compounds. The results show that the swelling and bending of the extrudate have a significant influence on the distortion of the interface and make its final shape different from that within the die, which is in accordance with previous experimental findings. The Weissenberg number (Wi) which represents the flow elasticity is proven to be a controlling factor of the interface shape. The numerical method proposed in this paper is also applied to an industrial profile and the agreement between the predicted extrudate profile and the experimentation is quite satisfactory. All of these

will contribute to a better understanding of the multilayer coextrusion flow of polymeric fluids.

ACKNOWLEDGMENTS

This work was funded by the Fundamental Research Funds for the Central Universities (No. WK2090050018) in China. We are grateful to Giti Tire Ltd for supplying the rubber compounds used in this study.

REFERENCES

1. Everage, A. E. *Trans. Sot. Rheol* **1973**, *I7*, 629.
2. Han, C. H. *J. Appl. Polym. Sci.* **1973**, *17*, 1289.
3. Lee, B. L.; White, J. L. *Trans. Soc. Rheol.* **1974**, *18*, 467.
4. Southern, J. H.; Ballman, R. L. *J. Polym. Sci.* **1975**, *13*, 863.
5. Everage, A. E. *Trans. Sot. Rheol.* **1975**, *19*, 509.
6. Takase, M.; Kihara, S.; Funatsu, K. *Rheol. Acta* **1998**, *37*, 624.
7. Anderson, P. D.; Dooley, J.; Meijer, H. E. H. *Appl. Rheol.* **2006**, *16*, 198.
8. Gupta, M. *Soc. Plast. Eng. Annu. Tech. (ANTEC) Papers* **2008**, *54*, 217.
9. Gupta, M. *Soc. Plast. Eng. Annu. Tech. (ANTEC) Papers* **2010**, *3*, 1688.
10. Yue, P.; Zhou, C.; Dooley, J.; Feng, J. J. *J. Rheol.* **2008**, *52*, 1027.
11. Borzacchiello, D.; Leriche, E.; Blottière, B.; Guillet, J. *J. Non-Newton. Fluid Mech.* **2013**, *200*, 52.
12. Borzacchiello, D.; Leriche, E.; Blottière, B.; Guillet, J. *J. Rheol.* **2014**, *58*, 493.
13. Chiou, J. Y.; Wu, P. Y.; Tsai, C. C.; Liu, T. J. *Polym. Eng. Sci.* **1998**, *38*, 49.
14. Karagiannis, A.; Hrymak, A. N.; Vlachopoulos, J. *Rheol. Acta* **1990**, *29*, 71.
15. Tanner, R. I. Engineering Rheology, 2nd ed.; Oxford University Press: Oxford, Clarendon, UK, **2000**.
16. Phan-Thien, N. *J. Rheol.* **1978**, *22*, 259.
17. Phan-Thien, N.; Tanner, R. I. *J. Non-Newton. Fluid Mech.* **1977**, *2*, 353.
18. Montes, S.; White, J. L. *J. Non-Newton. Fluid Mech.* **1993**, *49*, 277.
19. Kim, J. H.; Lyu, M. Y. *Polym. Eng. Sci.* **2014**, *54*, 2441.
20. Rajagopalan, D.; Armstrong, R. C.; Brown, R. A. *J. Non-Newton. Fluid Mech.* **1990**, *36*, 159.
21. Gifford, W. A. *Polym. Eng. Sci.* **1997**, *37*, 315.
22. ANSYS Polyflow User's Guide, Release 14.0; ANSYS Inc.: Canonsburg, PA, USA, **2011**.
23. Yang, C.; Li, Z. *Polym. Test.* **2014**, *37*, 45.
24. Song, H. J.; White, J. L.; Min, K.; Nakajima, N.; Weissert, F. C. *Adv. Polym. Technol.* **1988**, *8*, 431.
25. Leblanc, J. L. *Prog. Polym. Sci.* **2002**, *27*, 627.
26. Rippll, A.; Pittman, J.; Polynkin, A.; Sienz, J. *Rheol. Acta* **2007**, *46*, 847.
27. Graessley, W. W.; Glasscock, S. D.; Crawley, R. L. *Trans. Soc. Rheol.* **1970**, *14*, 519.
28. Liang, J. Z. *Polym. Test.* **2004**, *23*, 441.